Supporting Information for

Orientation-dependent Soft Plasmonics of Gold Nanobipyramid Plasmene Nanosheets

Runfang Fu,[1] Daniel E. Gómez,[2] Qianqian Shi,[1] Lim Wei Yap,[1] Quanxia Lyu,[1] Kaixuan Wang,[1] Zijun Yong,[1] & Wenlong Cheng[1] *

[1] Department of Chemical Engineering, Faculty of Engineering, Monash University, Clayton 3800, Victoria, Australia

[2] School of Science, RMIT University, Melbourne 3000, Victoria, Australia

* Correspondence to Prof Wenlong Cheng (wenlong.cheng@monash.edu)

Experimental Section

Materials. Gold (III) chloride trihydrate ($HAuCl_4 \cdot 3H_2O$, ≥99.9%), hexadecyltrimethylammonium bromide (CTAB), cetyltrimethylammonium chloride solution (CTAC, 25 wt % in H_2O), sodium borohydride ($NaBH_4$), L-ascorbic acid (AA), trisodium citrate (TC) and silver nitrate ($AgNO_3$) were obtained from Sigma-Aldrich. Ammonium hydroxide ($NH_3 \cdot H_2O$, 25 wt %), hydrogen peroxide (H_2O_2, 30 wt %) and chloroform was purchased from Merck Millipore. Tetrahydrofuran (THF) and hydrochloric acid (HCl, 32 wt %) was purchased from Thermal fisher scientific (Ajax Finechem). Thiol-functionalized polystyrene (PS, M_n = 50,000 and 20,000 g/mol) was obtained from Polymer Source. Polymethyl methacrylate (PMMA, 950 A6), was purchased from MicroChem Corp. Polydimethylsiloxane (PDMS, Sylgard 184) was from Dow corning. Indium tin oxide-coated glass slides (ITO glass, 30-60 Ω/sq) were purchased from South China Science & Technology Company Limited, China. Milli-Q water was obtained from Milli-Q Advantage A 10 water purification System. All materials were used without any further purification.

Synthesis of gold nanobipyramids (AuNBPs). AuNBPs were synthesised according to literature with small modifications.[1] Firstly, in order to synthesize seeds, 4.9 mL of 0.1 M CTAC, 5 mL of 10 mM TC, 0.1 mL of 25 mM $HAuCl_4$ and 0.25 mL 25 mM $NaBH_4$ were added subsequently into a 20 mL glass. The solution was mixed at room temperature for 2 min followed by keeping in an 80 ^oC water bath under 300 rpm stirring for 90 min. The seed solution was then cooled down to room temperature for further use. Then, the AuNBPs were grown by mixing 50 mL of 0.1M CTAB solution with 1 mL of 25 mM $HAuCl_4$, 0.5 mL of 10 mM $AgNO_3$, 1 mL of 1.0 M HCl, 0.4 mL of 0.1 M AA and 0.4 mL (for V-NBP plasmene nanosheets) or 0.1 mL (for H- and S-NBP plasmene nanosheets) of seed solution. After that, the mixed solution was kept in the 30 ^oC water bath for 2 hours. The as-prepared AuNBPs solution was collected

by centrifuging at 7830 rpm for 10 min. For purification of AuNBPs,[2] the above-synthesized AuNBPs were firstly redispersed in 70 mL of 80 mM CTAC and then 44 mL of 20 mM Ag NO_3 and 22 mL of 0.2 M AA were added. The mixed solution was kept in a 60 ^oC water bath for 4 hours under 500-rpm stirring. The solution was then cooled down to room temperature for the further use. The bimetallic Au/Ag product was collected by centrifuging at 6000 rpm for 10 min and then redispersed in 50 mL of 50 mM CTAB. The solution was kept undisturbed for 2 hours to precipitate the Au@Ag nanorods to the bottom of the container. After discarding the supernatant which mainly contains spherical-like nanoparticles, the precipitate was then redispersed in 20 mL of water and gently mixed with 3 mL of $NH_3 \cdot H_2O$ and 3 mL of H_2O_2. The mixed solution was kept undisturbed until the Ag shell was completely etched away. The clear supernatant was carefully taken out and centrifuged at 8200 rpm for 10 min. The highly pure Au NBPs were finally redispersed in 25 mL of 50 mM CTAB for further use.

Fabrication of AuNBP plasmene nanosheets. 4 mL (for S-NBP) or 5 mL (for V-NBP and H-NBP) of AuNBPs aqueous solution were diluted to 10 mL with MQ water, centrifuged at 8200 rpm for 10 min and finally redispersed in 4 mg/mL PS in THF solution. PS with molecular weight of M_n = 50,000 g/mol was used for H-NBP plasmene nanosheets and M_n = 20, 000 g/mol was for V-NBP and S-NBP plasmene nanosheets. The AuNBPs solution were kept undisturbed overnight to finish the ligand exchange. The PS-capped AuNBPs were washed with THF for 2 times and chloroform once to remove the residual PS ligands. The final PS-capped AuNBPs in chloroform was concentrated to about 10 μL after centrifuge. Finally, one drop of concentrated PS-capped AuNBPs solution was spread on the surface of a convex-shaped water droplet sitting on a PMMA-coated Si wafer (or ITO glass). After the water completely evaporated, a continuous monolayer AuNBP nanosheet was formed on the substrate. For PMMA-coated Si wafer, a drop of PMMA was spin coated on a clean Si wafer at 3000 rpm for 45s and then baked at 180 °C for 2 min.

Embed AuNBP plasmene in PDMS. To partially embed AuNBP plasmene into PDMS, the sacrificial PMMA was used as substrate for growing the plasmene nanosheets. The above-prepared AuNBP plasmene nanosheets on PMMA-coated Si wafer were treated by air plasma which generated ionic species that are high reactive with organic compounds such as PS ligands. Under our experimental condition, a 5 min plasma treatment was applied under high radio frequency power (RF) using Harrick Plasma Cleaner PDC-002-HP. This ensured partial removal of PS ligands from top side of AuNBP plasmene with gold surface exposed. After air plasma treatment, a thin layer of PDMS (mixed with curing agent at weight ratio of 10:1) was spin-coated at 400 rpm for 30s on surface of plasmene nanosheets, which was followed by curing at 70 ^{o}C in an oven for 30 min. The partially exposed gold surfaces could promote bonding to PDMS, hence, offering strong adhesion. After the PDMS was fully cured and cooled down to room temperature, the whole sample on Si wafer was immersed in an acetone-contained beaker to dissolve the sacrificial PMMA layer. Then the free-standing PDMS-supported plasmene nanosheets could be obtained.

Modeling of fractional resonance energy change. The Electrostatic Eigenmode Model (EEM) was applied to model the strain-induced energy change in NBP plasmene system. We considered the interaction of point dipoles located along a straight line. According to the EEM, the localised surface plasmon resonances are due to particle-particle coupling, which can be approximated as being dominated by dipole-dipole coupling between near-neighbours. This coupling takes the form:

$$G \propto \frac{1}{d^3}\{3\left(\vec{p}_i \cdot \hat{d}_{ij}\right)\left(\vec{p}_j \cdot \hat{d}_{ij}\right) - \left(\vec{p}_i \cdot \vec{p}_j\right)\}$$

Where d is the separation distance between dipole $\vec{p}_{ij}$. We assume all dipoles to be located along a line, i.e. $\vec{d} = d \cdot \hat{x}$. In the same coordinate system, each dipole moment is written as: $\vec{p}_i = p\left(\cos(\theta_i)\ \hat{x} + \sin(\theta_i)\ \hat{y}\right)$, and we furthermore assume all particles to be identical:

$|\vec{p}_i| = |\vec{p}_j| = p$. Within these approximations, then the fractional energy change ΔE is expressed as: $\Delta E = \frac{G(d)-G(d_o)}{G(d_o)} = \left(\frac{d_o}{d}\right)^3 \frac{f(\theta)}{f(\theta_o)} - 1$, where $f(\theta) = 3\ \cos(\theta)^2 - 1$ contains the orientational information of the dipoles. We then adjusted the fitting parameters including the maximum distance under stretching and the initial orientation angle (θ_o) and the final orientation angle (θ) to calculate the fractional energy change.

It is worth to mention that if we assume the angles do not change with an applied strain (that is, we attempt to explain the results with only increases in separation) then we obtain:

$$\frac{\delta E}{E_o} = \frac{G(d)-G(d_o)}{G(d_o)} = \left(\frac{d_o}{d}\right)^3 - 1,$$

which implies that $\frac{\delta E}{E_o}$ always decreases with increases in separation distance d, contrary to experiment cases such as the ones shown in Figure 4e and Figure S20-22.

Characterization. The morphology of plasmene nanosheets was characterized by scanning electron microscope (SEM, FEI Helios Nanolab 600 focused ion beam (FIB)-SEM operating at voltage of 5 kV and current of 86 pA). An Agilent 8453 UV−vis spectrophotometer was used to record the absorption spectra and a J&M MSP210 microscope spectrometry system under a 20× objective was used to record the extinction spectra of plasmene nanosheets. The acquired area for extinction spectra of plasmene nanosheets is 6 μm×6 μm. The polarization-dependent UV-vis spectra were measured using an upright microscope (Nikon LV100), coupled to a spectrograph (HR4000, Ocean Optics) using a 50× objective. The polarizer is located between the objective and detector. The stretching and releasing cycling test was carried on motorized moving stages (THORLABS Model LTS150/M) which were connected to a computer-based user interface (Thorlabs APT user). The cyclic stretching speed was about 2 mm/s. Each time after 50 cycles of cyclic stretching, the extinction spectra of plasmene

nanosheets were recorded by J&M MSP210 microscope spectrometry system under a 20× objective.

Figures

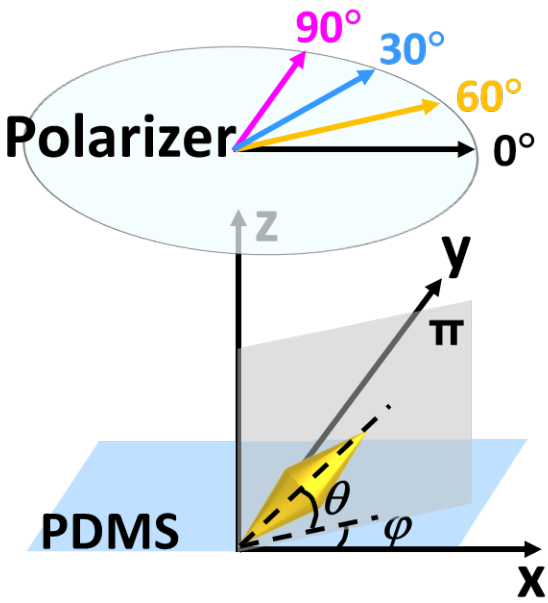

Figure S1 Scheme of S-NBP irradiated by light. Two perpendicular planes were introduced for convenient explanation: xy-plane (where the air-PDMS interface is) and plane π (where the S-NBP is). θ is orientation angle of S-NBP. φ is the azimuth angle of S-NBP. Positive z-axis is the incident light direction. The x-axis is the stretching direction.

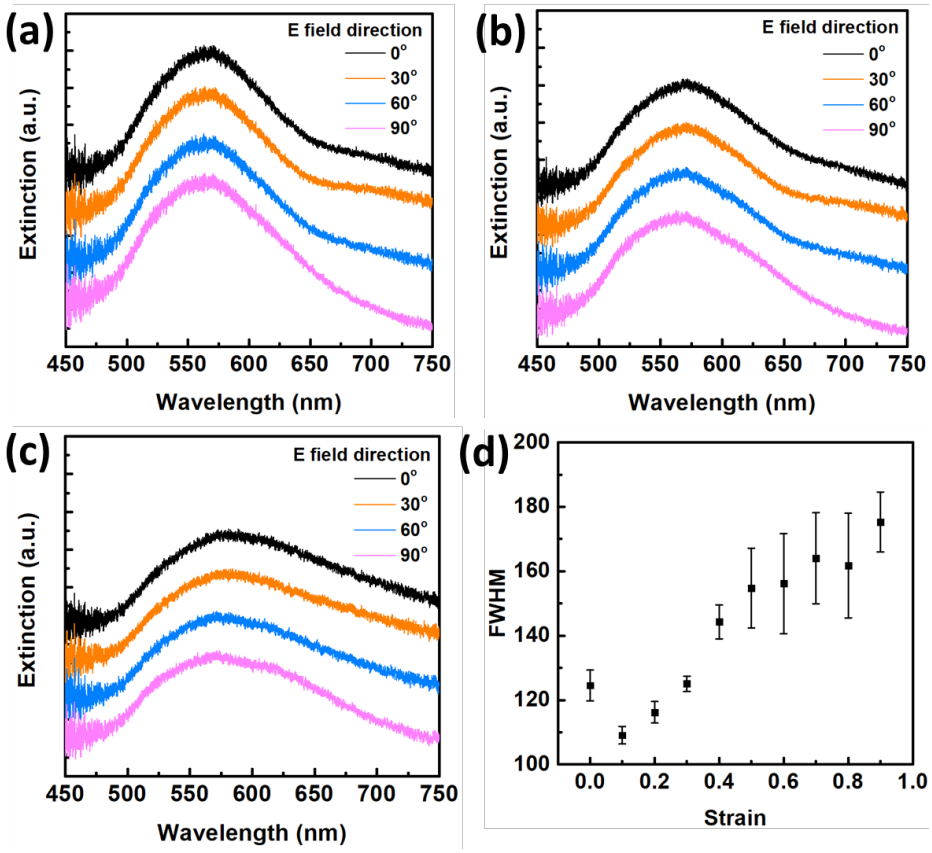

Figure S2 Representative extinction spectra of V-NBP plasmene under different strains (a) 10%, (b) 30% and (c) 60%. (d) The full width at half maximum (FWHM) of extinction spectra at different strains.

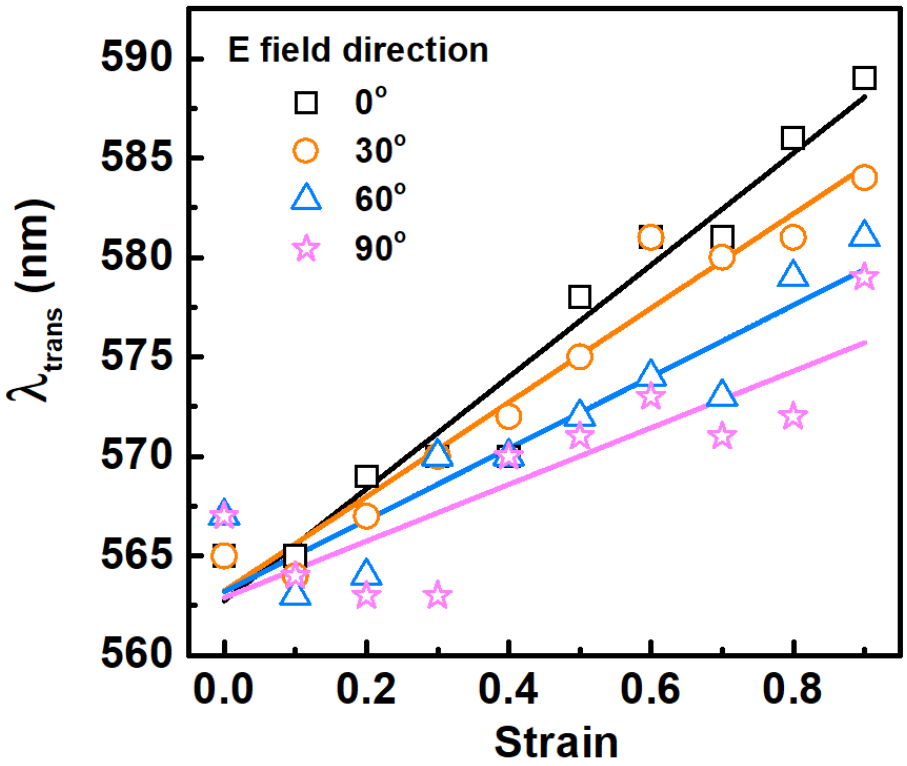

Figure S3 Strain-induced transverse LSPR peak evolution of V-NBP plasmene collected at different polarized angles.

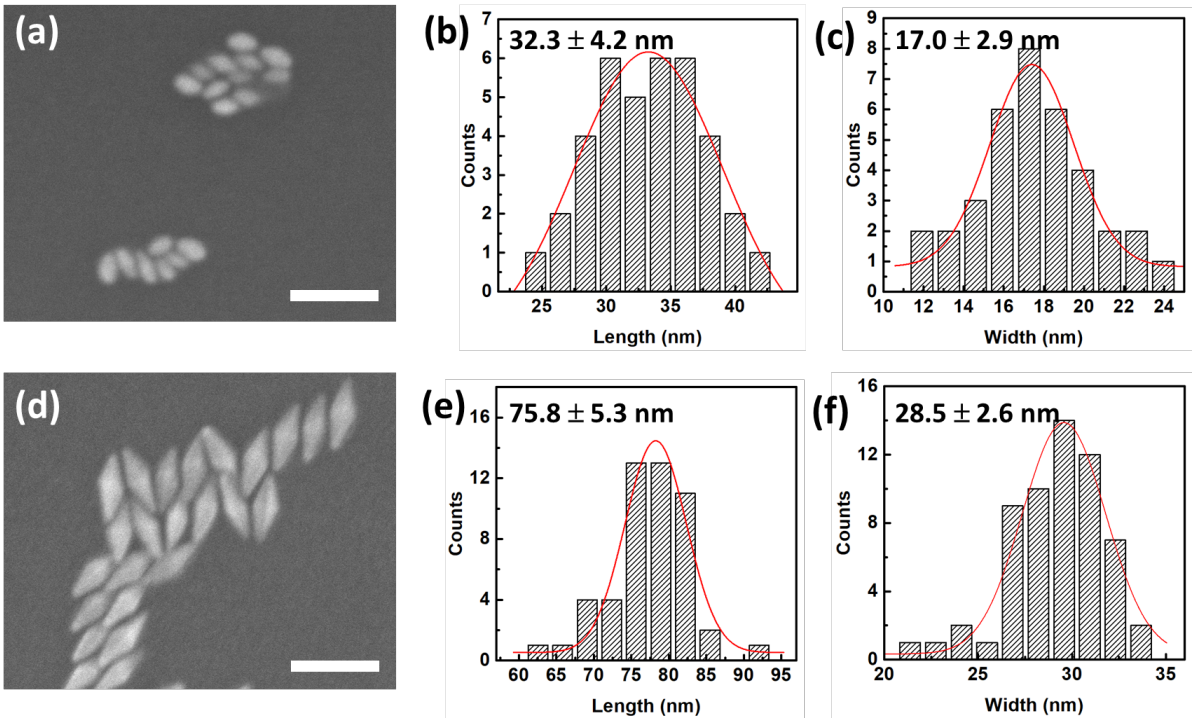

Figure S4 SEM images and size distribution of discrete AuNBP on Si wafer: (a-c) AuNBP used for V-NBP plasmene; (d-f) AuNBP used for H-NBP and S-NBP plasmenes.

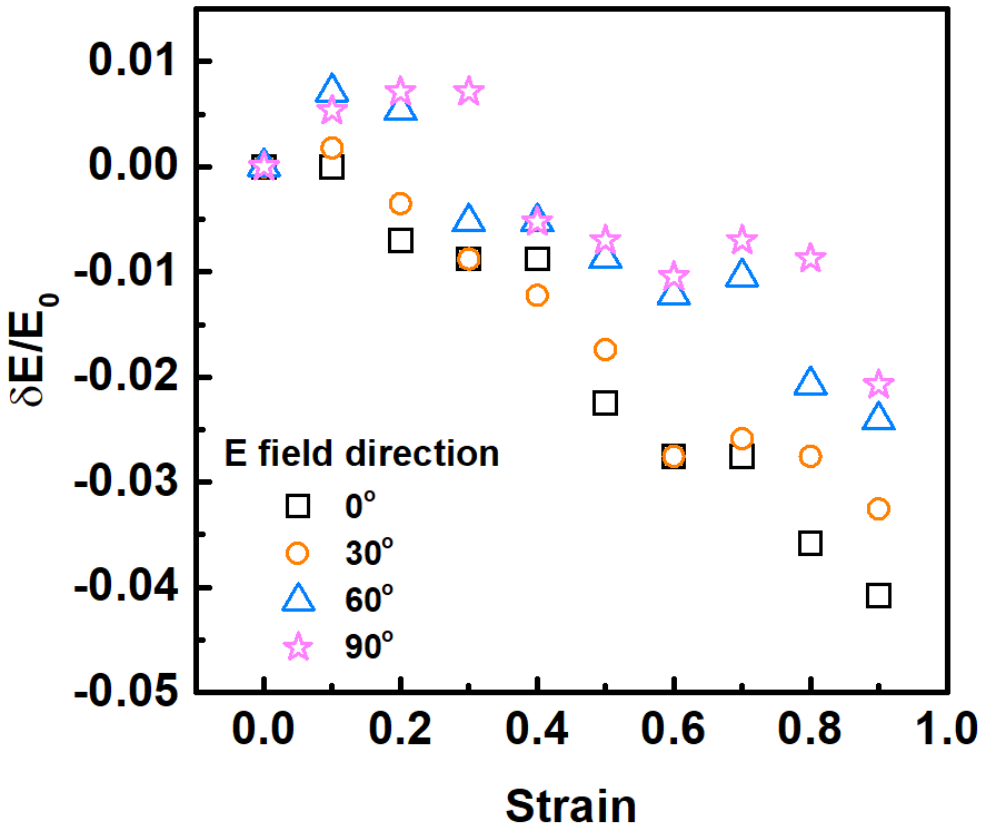

Figure S5 Fractional energy change of V-NBP plasmene under strains (δE is the energy change relative to energy at no strain E_0)

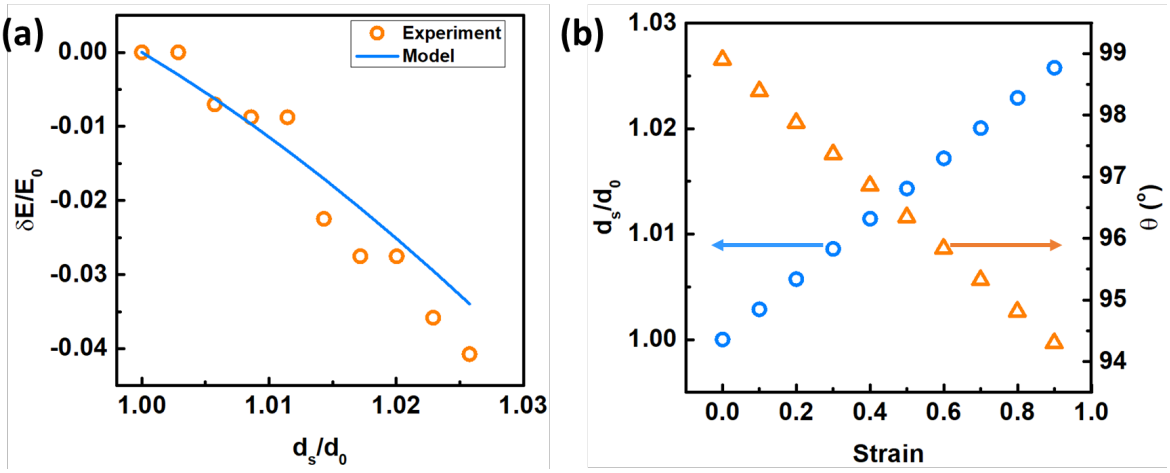

Figure S6 (a) Modeled fractional energy change of V-NBP plasmene with (b) assumption of separation and orientation change with 0°-polarization. (δE is the energy change relative to energy at no strain E_0, d_0 is the assumed initial separation between V-NBP)

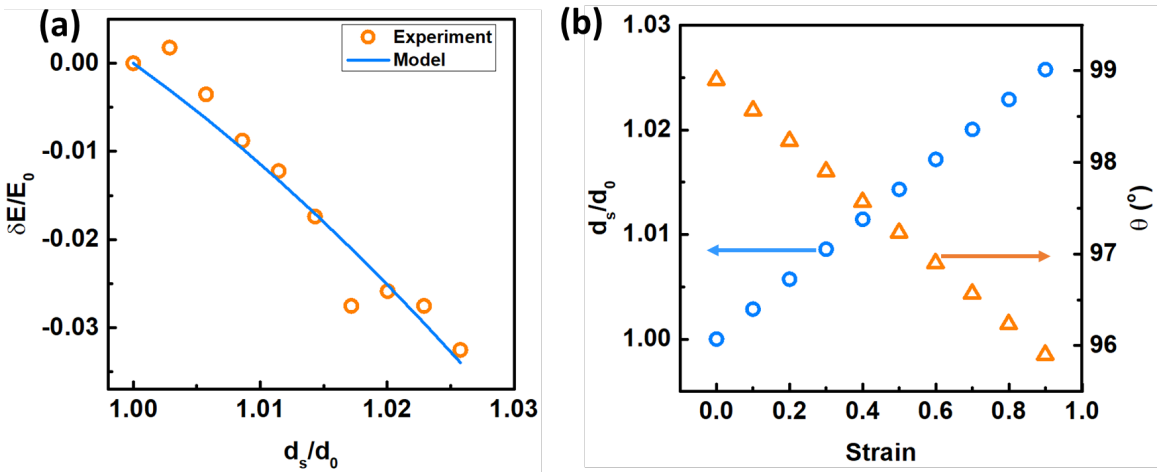

Figure S7 (a) Modeled fractional energy change of V-NBP plasmene with (b) assumption of separation and orientation change with 30°-polarization. (δE is the energy change relative to energy at no strain E_0, d_0 is the assumed initial separation between V-NBP)

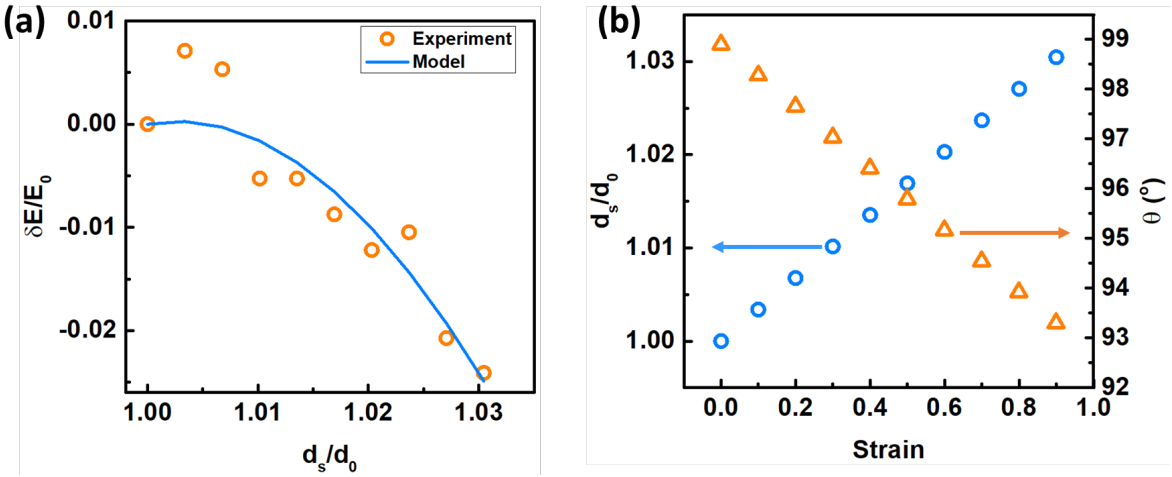

Figure S8 (a) Modeled fractional energy change of V-NBP plasmene with (b) assumption of separation and orientation change with 60°-polarization. (δE is the energy change relative to energy at no strain E_0, d_0 is the assumed initial separation between V-NBP)

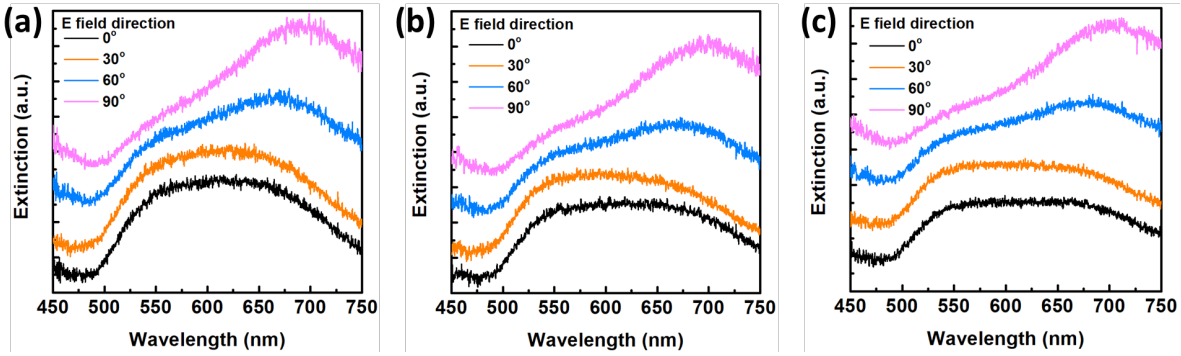

Figure S9 Representative extinction spectra of S-NBP plasmene under different strains (a) 10%, (b) 30% and (c) 60%.

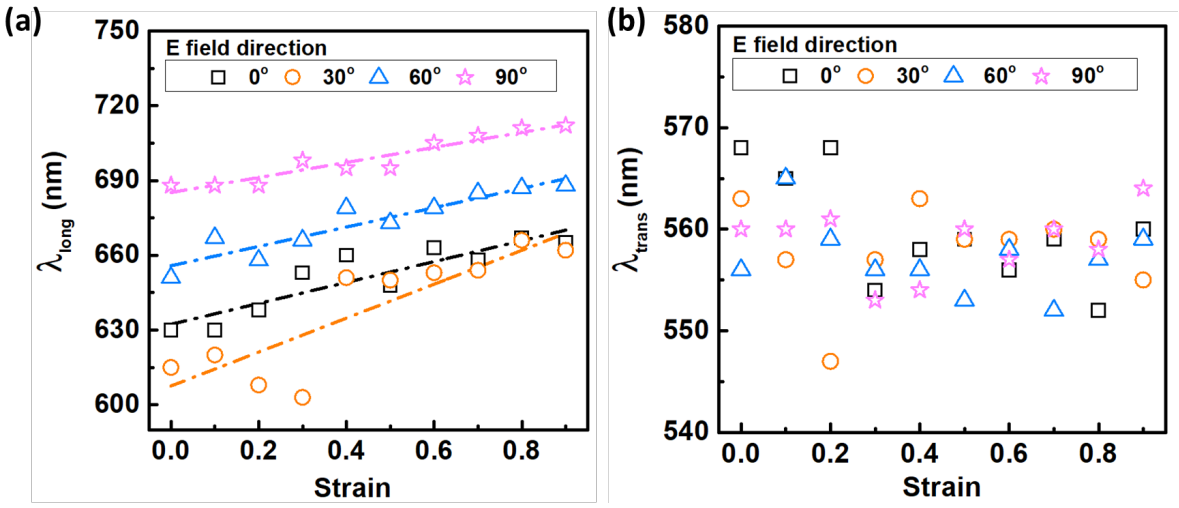

Figure S10 Strain-induced evolution of LSPR peak of S-NBP plasmene: (a) longitudinal peak, (b) transverse peak.

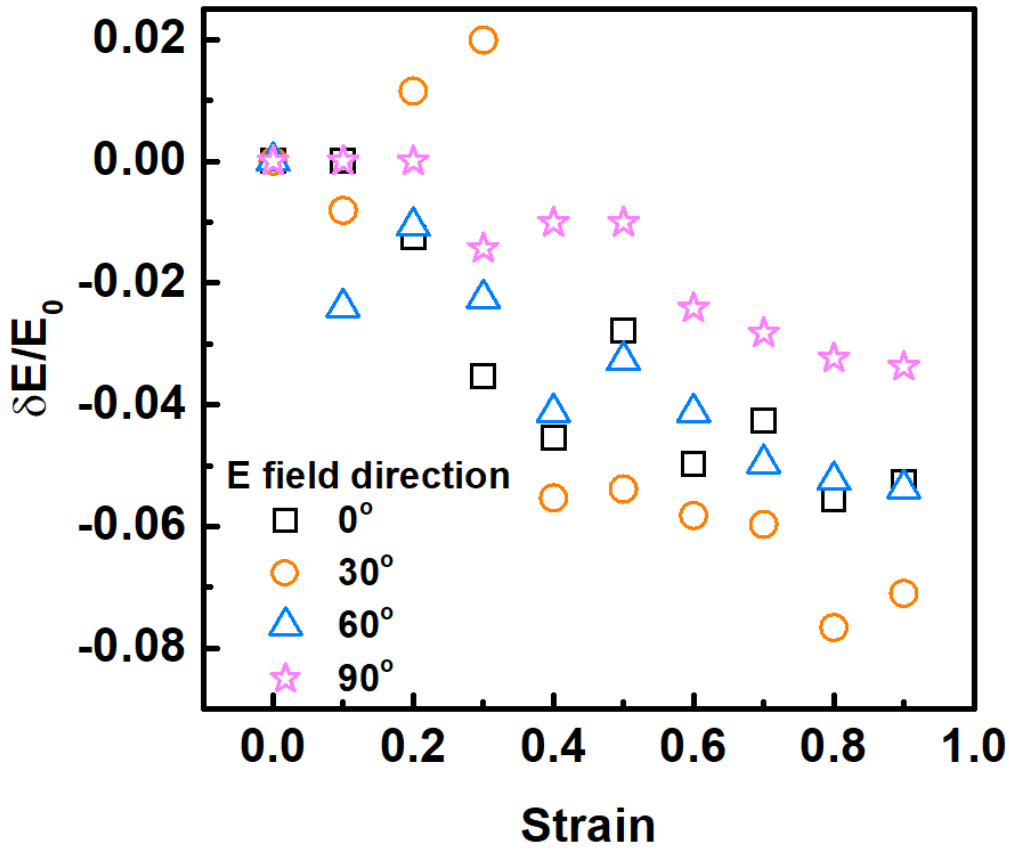

Figure S11 Longitudinal fractional energy change of S-NBP plasmene under strains (δE is the energy change relative to energy at no strain E_0)

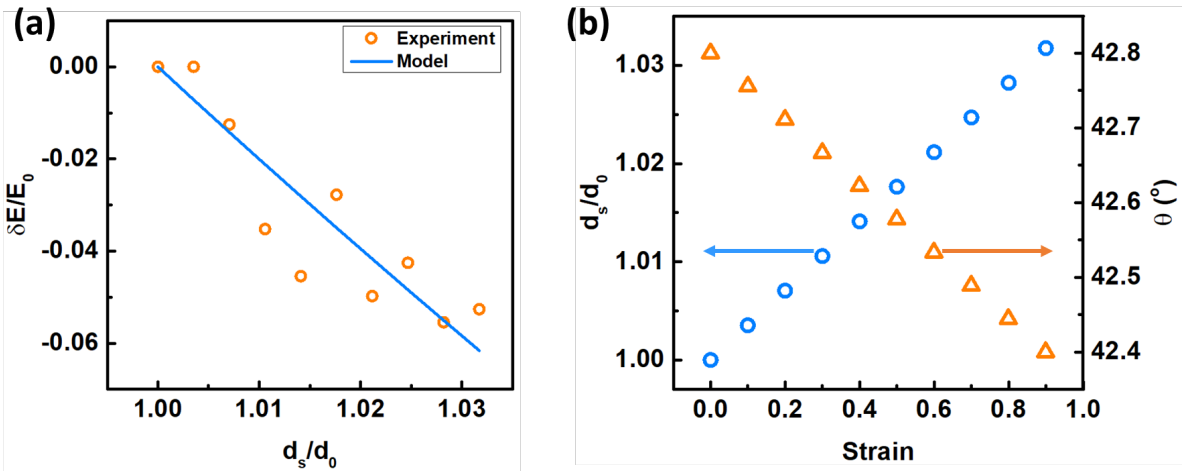

Figure S12 (a) Modeled fractional energy change of S-NBP plasmene with (b) assumption of separation and orientation change with 0°-polarization. (δE is the energy change relative to energy at no strain E_0, d_0 is the assumed initial separation between S-NBP)

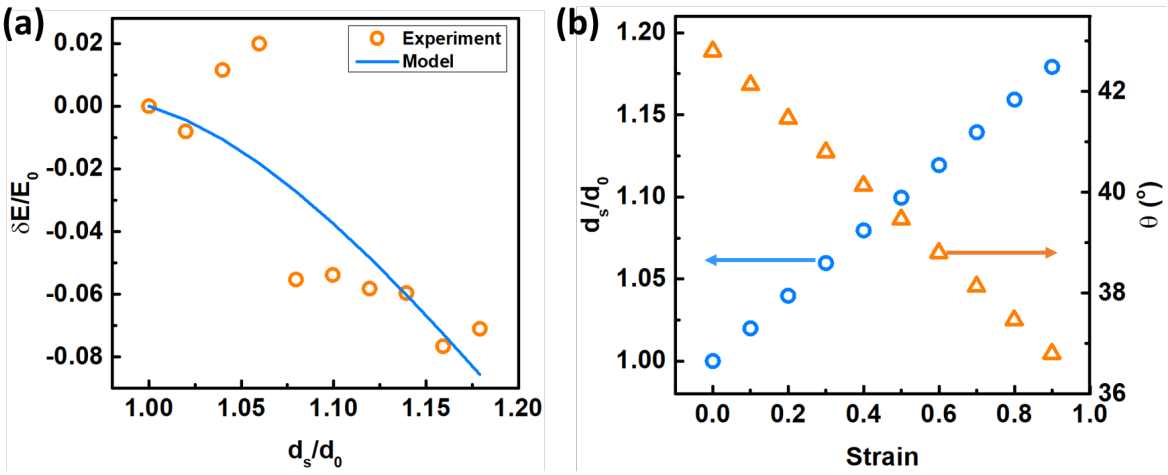

Figure S13 (a) Modeled fractional energy change of S-NBP plasmene with (b) assumption of separation and orientation change with 30°-polarization. (δE is the energy change relative to energy at no strain E_0, d_0 is the assumed initial separation between S-NBP)

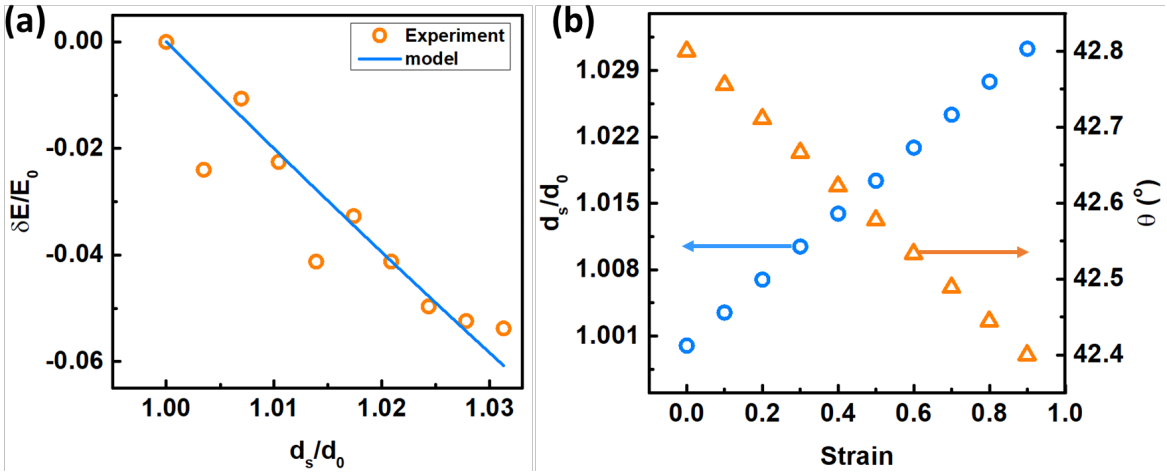

Figure S14 (a) Modeled fractional energy change of S-NBP plasmene with (b) assumption of separation and orientation change with 60°-polarization. (δE is the energy change relative to energy at no strain E_0, d_0 is the assumed initial separation between S-NBP)

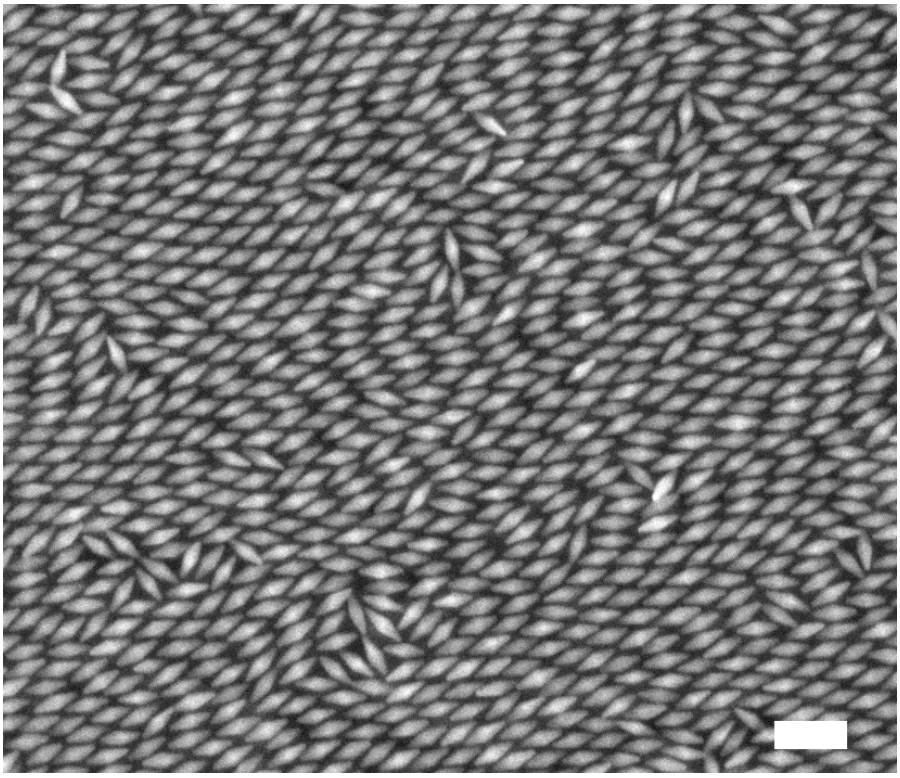

Figure S15 SEM images of H-NBP plasmene on Si wafer (Scale bar: 100 nm)

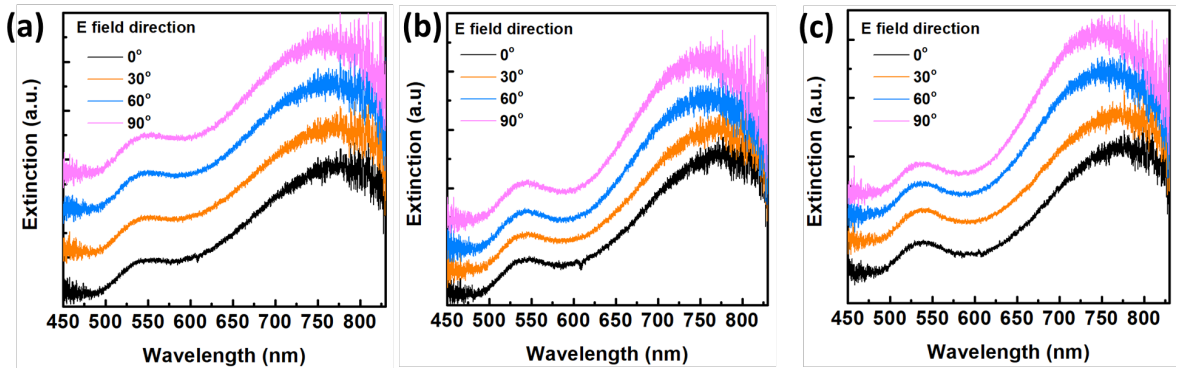

Figure S16 Representative extinction spectra of horizontal AuNBP plasmene under different strains (a) 10%, (b) 30% and (c) 60%.

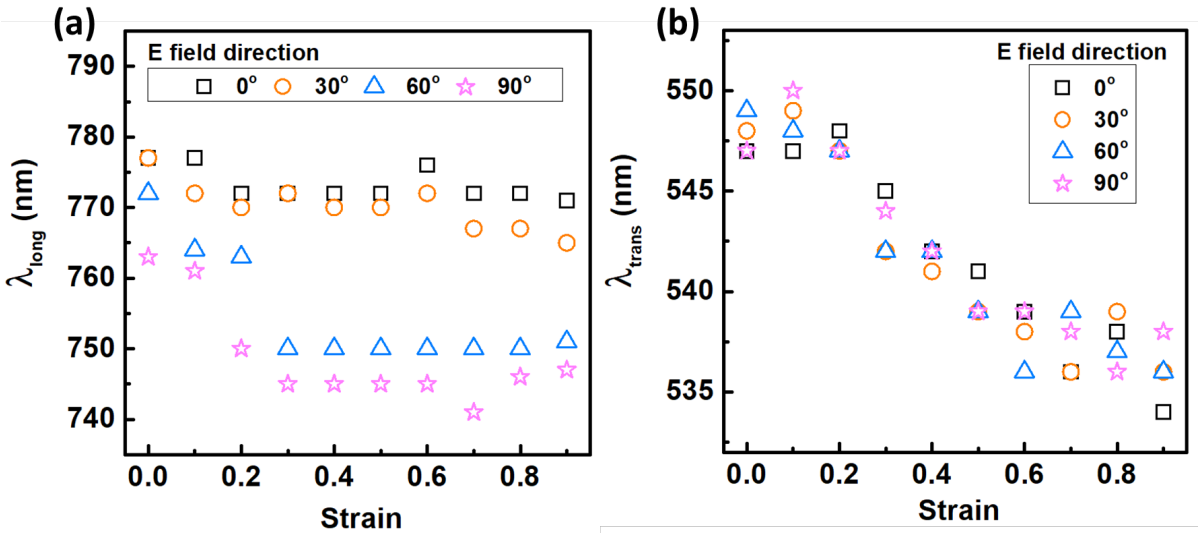

Figure S17 Strain-induced evolution of plasmon resonance peak of horizontal AuNBP plasmene detected with polarizer: (a) longitudinal peak, (b) transverse peak.

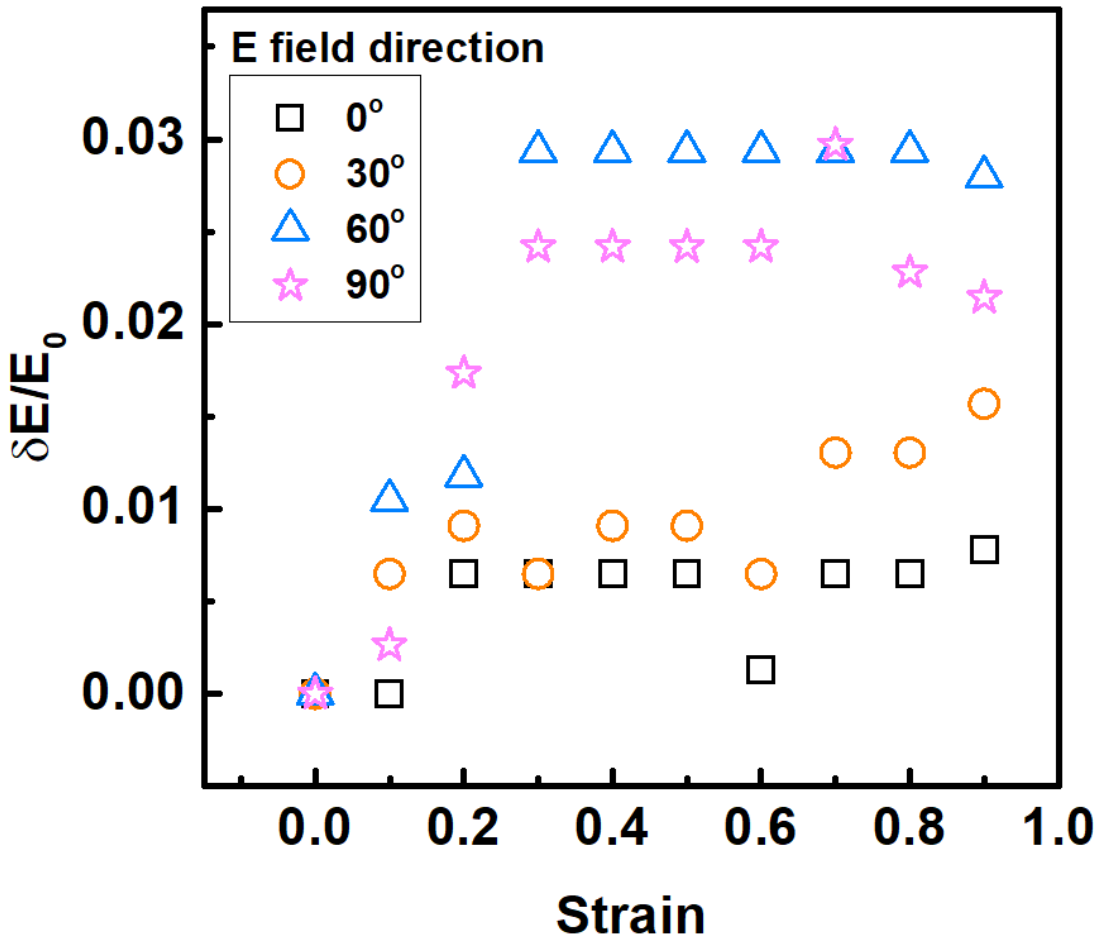

Figure S18 Longitudinal fractional energy change of horizontal AuNBP plasmene under strains. (δE is the energy change relative to energy at no strain E_0)

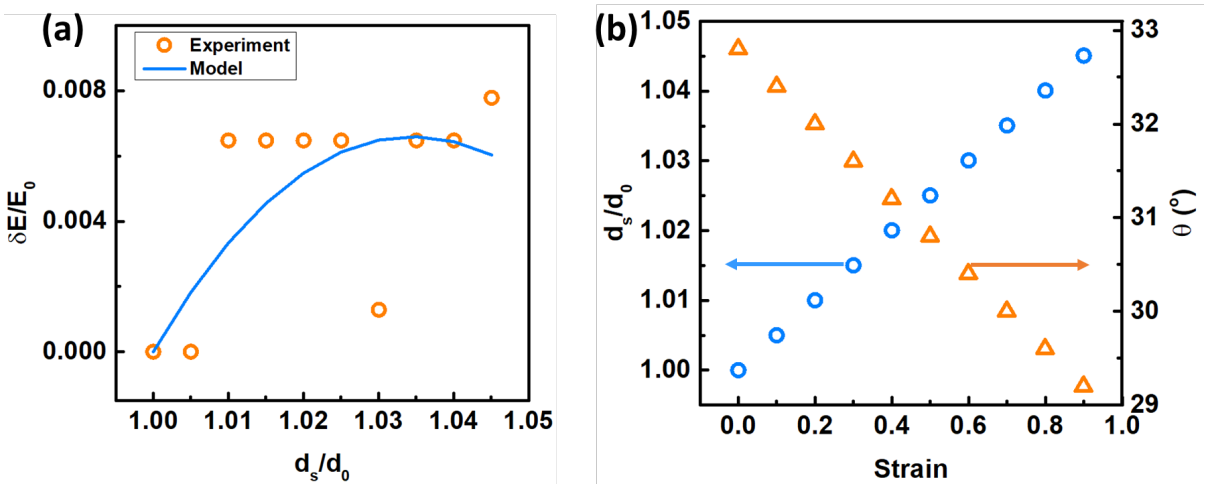

Figure S19 (a) Modeled fractional energy change of horizontal AuNBP (H-NBP) plasmene with (b) assumption of separation and orientation change with 0°-polarization. (δE is the energy change relative to energy at no strain E_0, d_0 is the assumed initial separation between H-NBP)

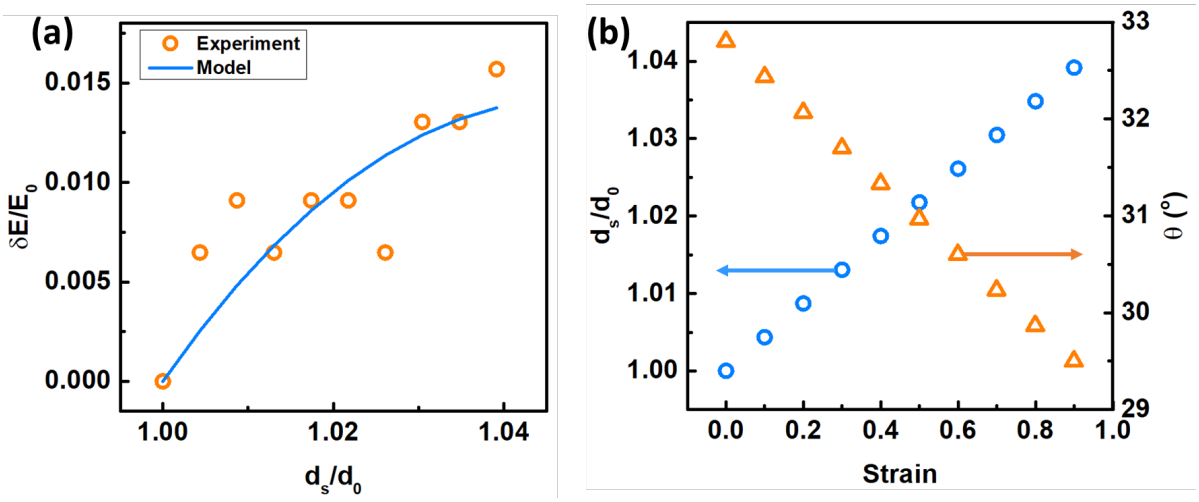

Figure S20 (a) Modeled fractional energy change of horizontal AuNBP (H-NBP) plasmene with (b) assumption of separation and orientation change with 30°-polarization. (δE is the energy change relative to energy at no strain E_0, d_0 is the assumed initial separation between H-NBP)

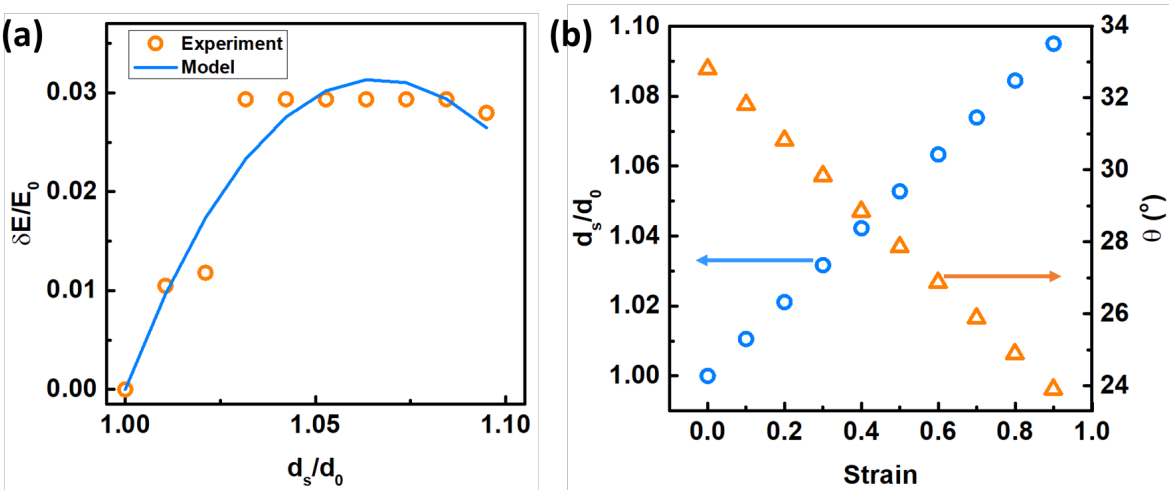

Figure S21 (a) Modeled fractional energy change of horizontal AuNBP (H-NBP) plasmene with (b) assumption of separation and orientation change with 60°-polarization. (δE is the energy change relative to energy at no strain E_0, d_0 is the assumed initial separation between H-NBP)

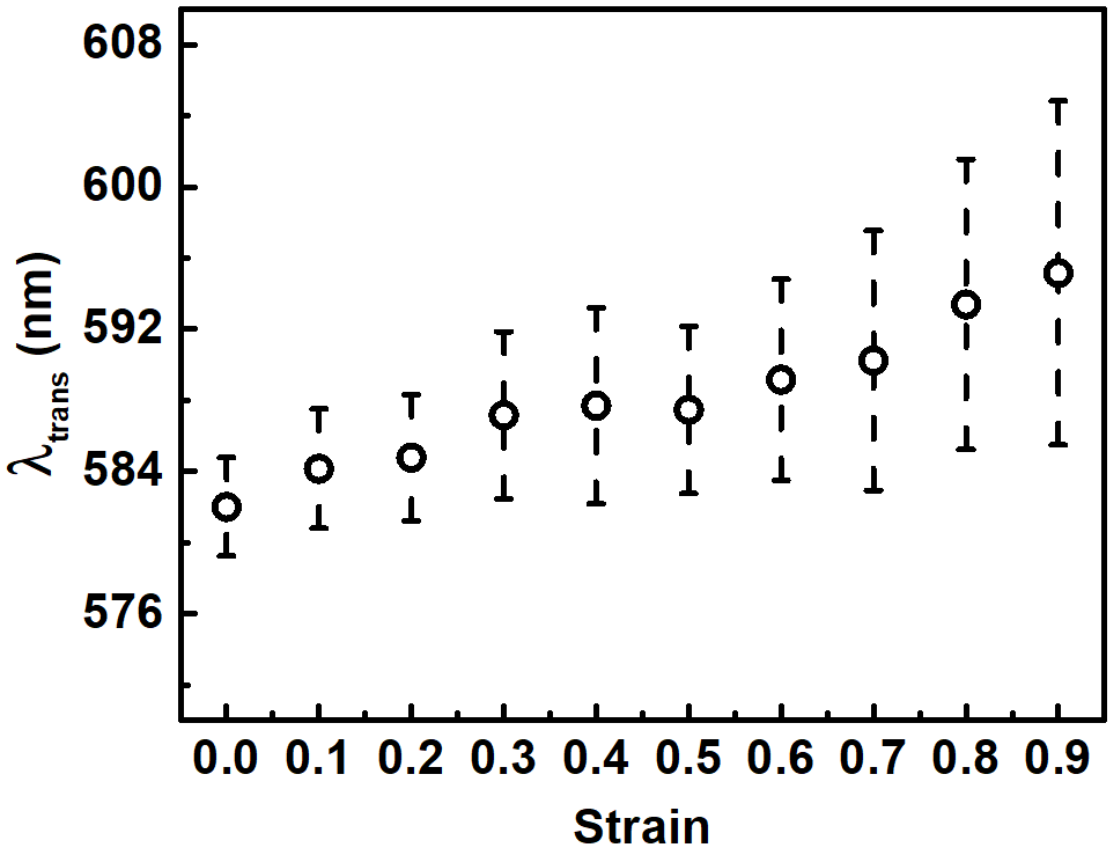

Figure S22 Systematic investigation of strain-induced transverse LSPR peak evolution of V-NBP plasmene.

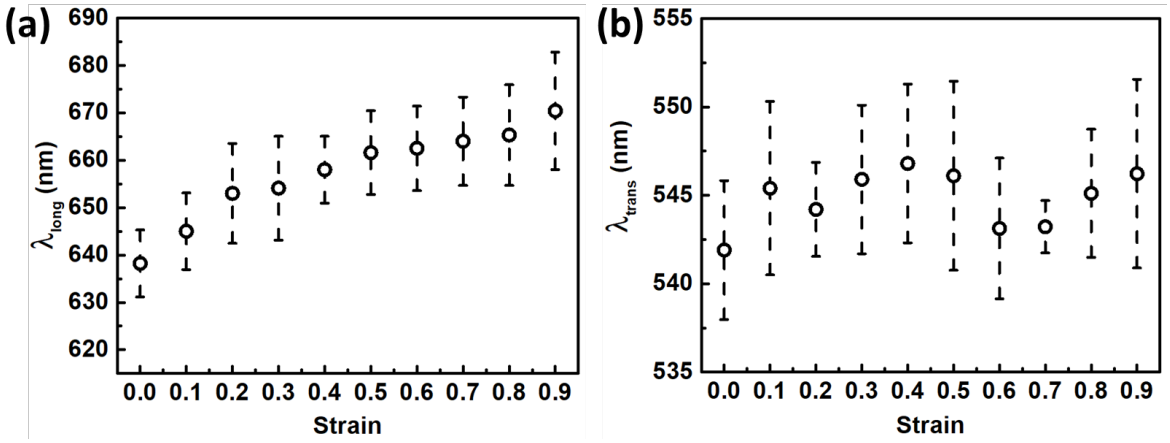

Figure S23 Systematic investigation of strain-induced (a) longitudinal and (b) transverse LSPR peak evolution of S-NBP plasmene.

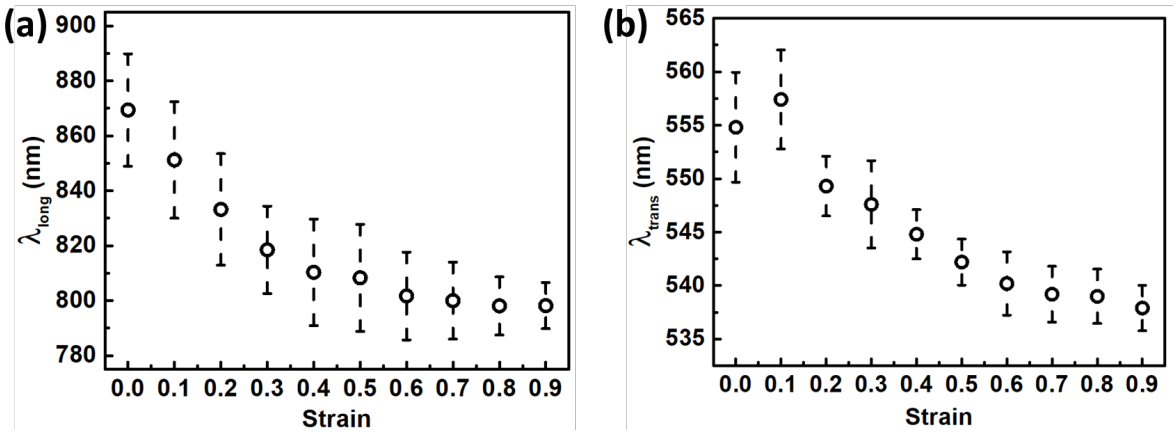

Figure S24 Systematic investigation of strain-induced (a) longitudinal and (b) transverse LSPR peak evolution of H-NBP plasmene.

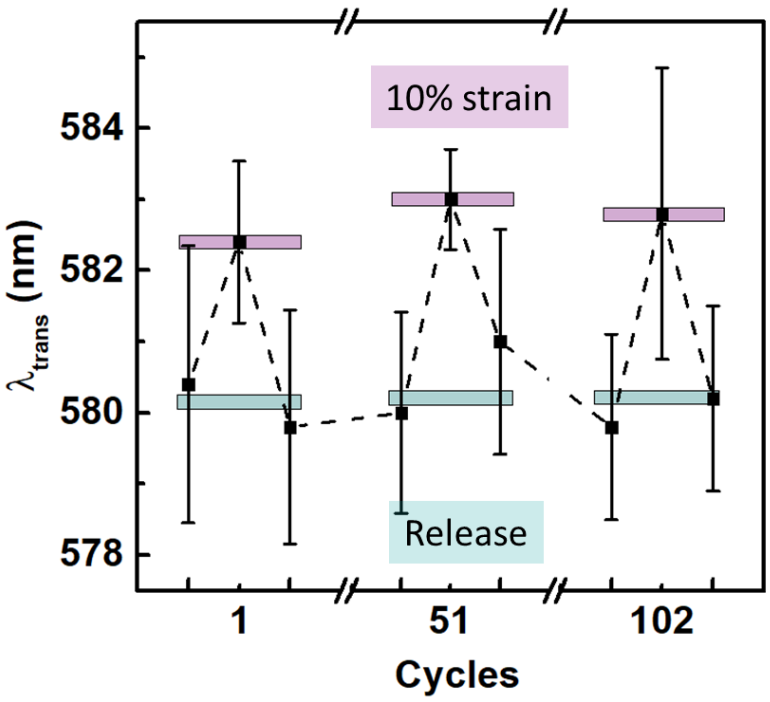

Figure S25 Durability of transverse LSPR mode of V-NBP plasmene nanosheets under stretch-release cycles.

References

1. Sánchez-Iglesiass, A.; Winckelmans, N.; Altantzis, T.; Bals, S.; Grzelczak, M.; Liz-Marzán, L. M. High-yield seeded growth of monodisperse pentatwinned gold nanoparticles through thermally induced seed twinning. *J. Am. Chem. Soc.* **2017,** 139, (1), 107-110.

2. Li, Q.; Zhuo, X.; Li, S.; Ruan, Q.; Xu, Q.-H.; Wang, J. Production of Monodisperse Gold Nanobipyramids with Number Percentages Approaching 100% and Evaluation of Their Plasmonic Properties. *Adv. Opt. Mater.* **2015,** 3, (6), 801-812.